Further studies of a Cr^{3+}-like centre in GaP

1998 J. Phys.: Condens. Matter 10 10019

(http://iopscience.iop.org/0953-8984/10/44/010)

J. Phys.: Condens. Matter **10** (1998) 10019–10033. Printed in the UK PII: S0953-8984(98)94716-6

Further studies of a Cr^{3+}-like centre in GaP

A Erramli†‖, Y-M Liu‡, A-M Vasson†¶, A Vasson†, M Darcha†, M El-Metoui†$^{+}$, B Clerjaud§, C A Bates‡ and J L Dunn‡

† LASMEA*, Physique 4, Université Blaise-Pascal Clermont-Ferrand II, 63177 Aubière Cédex, France

‡ School of Physics and Astronomy, University of Nottingham, University Park, Nottingham NG7 2RD, UK

§ Laboratoire d'Optique des Solides, Case Courrier 80, Université Pierre et Marie Curie, 4 Place Jussieu, F-75252 Paris Cédex 05, France

Received 2 June 1998, in final form 4 August 1998

Abstract. A centre in GaP having a Cr^{3+}-like behaviour has been studied both experimentally and theoretically. It was identified originally by thermally detected (TD) EPR experiments carried out at liquid helium temperatures and correlated with the optical absorption 1.03 eV zero phonon line from the isolated substitutional Cr^{3+} ion. Subsequent TD-EPR experiments on different types of samples and sub-band-gap illumination effects show that, although the centre is Cr^{3+}-like, it can not be the isolated Cr^{3+} ion. A theoretical model is proposed in which this Cr^{3+}-like ion is described by a strain-stabilized $T \otimes (e \oplus t_2)$ Jahn–Teller (JT) model associated with wells that have orthorhombic symmetry in the potential energy surface. On fitting the isofrequency curves to all the relevant TD-EPR data, values for the second-order JT reduction factors are obtained which indicate that this Cr^{3+}-like centre is strongly coupled to its surroundings. The electronic structure of this centre has still to be established.

1. Introduction

The GaAs:Cr^{3+} system has been studied extensively by electron paramagnetic resonance (EPR) and corresponding theoretical models have become reasonably well established (e.g. Krebs and Stauss 1977, Clerjaud 1985, Parker *et al* 1990). In contrast, the Cr^{3+} ion in GaP is relatively difficult to identify and interpretations of the experimental data are somewhat confusing. Many optical absorption (OA) and photoluminescence (PL) experiments on chromium-doped GaP systems have been carried out (e.g. Dean 1973, Kaufmann and Koschel 1978, Eaves *et al* 1980, Williams *et al* 1982), concentrating on the 1.03 eV zero-phonon line (ZPL). Tetragonal strains were assumed to be responsible for the tetragonal symmetry observed by Eaves *et al* (1980) in their high-field optical Zeeman measurements. However, the centre responsible for this ZPL was not clearly identified until Eaves *et al* (1985) assigned this line to the internal transitions between the $^4T_1$ ground state and the $^4T_2$ excited state of a Cr^{3+} ion.

EPR studies of samples of chromium-doped GaP were undertaken by Dunn *et al* (1986) using thermally detected (TD) procedures. Details of this technique are given in

‖ Now at: LSM, Faculté des Sciences Semlalia, Université Cadi-Ayyad, BP S15, 40001-Marrakech, Morocco.
¶ Deceased.
$^{+}$ Now at: Faculté des Sciences et Techniques de Tanger, Departement de Physique, BP 416, Tangiers, Morocco.
* UMR CNRS No 6602

0953-8984/98/4410019+15$19.50

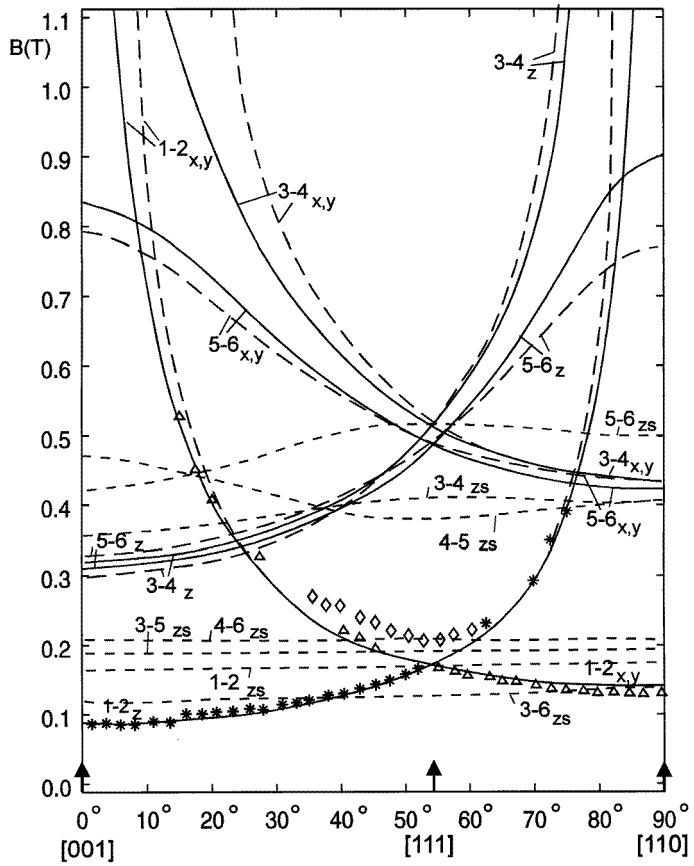

Figure 1. The experimental isofrequency data for a frequency of 8.7 GHz for $\boldsymbol{B}$ in the $(1\bar{1}0)$ plane constructed from the data given in Dunn *et al* (1986) and Darcha *et al* (1987) for the Cr^{3+}-like resonances *, △ and ◊. The theoretical isofrequency curves of Dunn *et al* (1986) for tetragonally strained stabilized sites are shown and identified by - - - -, —— and – – – for tetragonal strains of -50, -20 cm^{-1} and zero respectively. The transitions are identified by the levels (lowest number lowest) between which the transitions occur; the subscripts x, y, z label the symmetry of the tetragonal sites and 'zs' stands for the 'zero-strain' sites.

Vasson *et al* (1993). In order to model this system, Dunn *et al* (1986) suggested that the ion responsible for the observed TD-EPR spectra was Cr^{3+} and thus they introduced an effective Hamiltonian describing the $^4T_1$ ground state of this ion. To account for the angular dependence of the isofrequency spectra, a strain-stabilized T ⊗ e dynamic Jahn–Teller (JT) model was proposed in which tetragonal strains dominate. The TD-EPR data were correlated with the Cr^{3+} 1.03 eV ZPL in zero magnetic field by using the ground state splittings found from the optical experiments in the effective Hamiltonian. This model was then used to predict the TD-EPR isofrequency curves for both strain-stabilized and zero-strain sites and agreement between some of the experimental points and theoretical predictions was obtained.

Additional TD-EPR and TD-OA experiments were subsequently carried out on other samples to elucidate further the properties of chromium impurities in GaP. In particular, Houbloss *et al* (1987) studied photo-induced changes in both the TD-OA and TD-EPR

spectra in an attempt to correlate the changes in the two types of spectrum. Simultaneously, Darcha *et al* (1987) studied the frequency dependence of the TD-EPR spectra together with new angular-dependent measurements. From an analysis of the resonances attributed to strain-stabilized sites, it was concluded that the results were consistent with a JT ion with a spin $S = 3/2$ and having a g-value near to 2. Again, it was supposed that this ion was substitutional Cr^{3+}. However, it was recognized that the correlation between the 1.03 eV ZPL in the OA and TD-EPR spectra was strictly valid only for a magnetic field $\boldsymbol{B}$ along the [111] direction. No definitive conclusion was reached as to whether the ion responsible for the TD-EPR spectra is indeed chromium and, if so, whether it occupies an isolated substitutional site or whether it forms part of a complex. The connection between the 1.03 eV ZPL and the TD-EPR spectra was thereby weakened by these results.

During the last few years, there has been renewed interest in complex formation in insulating and semiconducting crystals. Consequently, we have re-examined the GaP:Cr system and carried out further experiments on many other samples. These results, to be described below, have cast further doubt on the original correlation between the 1.03 eV ZPL and the TD-EPR lines attributed to a substitutional Cr^{3+} ion. In parallel with these more recent experiments, a much more sophisticated JT theory has been developed for strongly coupled systems in which the importance of second-order reduction factors has been emphasized. It is necessary, therefore, to re-examine also all aspects of the original model in order to give a more satisfactory and consistent account of both the old and new experimental data using improved theoretical models. In particular, we are in a position now to consider the application of a $T \otimes (e \oplus t_2)$ strain-stabilized JT model instead of the original $T \otimes e$ model to account for the TD-EPR data as suggested by Darcha *et al* (1987). These new experimental data and revised modelling form the subject of the present paper; a preliminary discussion has been given very recently by Vasson *et al* (1997).

Section 2 summarizes some of the existing TD-EPR data and sections 3 and 4 describe the results obtained from more recent experiments including the effects of illumination on the resonance spectra. Section 5 describes the strain-stabilized $T \otimes (e \oplus t_2)$ JT model and gives analytical expressions for the spin Hamiltonian parameters. Values for these parameters are obtained by fitting to the experimental data. Finally, the implications of these results and the theory are discussed in section 6.

2. Background information

2.1. A summary of some previous TD-EPR results

Dunn *et al* (1986) deduced that, for negative strains of magnitudes greater than about 20 cm^{-1}, the TD-EPR spectra would arise from strain-stabilized sites of tetragonal symmetry. This conclusion was reached from an analysis of the diagram showing the dependencies of the energy levels associated with the $^4T_1$ ground-state-type on E-type strain deduced from an analysis of the 1.03 eV ZPL. Figure 1, giving the experimental isofrequency curves at 8.7 GHz for a magnetic field $\boldsymbol{B}$ lying within the $(1\bar{1}0)$ plane, has been constructed from the results reported in Dunn *et al* (1986) and Darcha *et al* (1987). It shows the isofrequency curves calculated for three values of the strain (namely 0, -20 cm^{-1} and -50 cm^{-1}) together with selected sets of data points for the centre having a Cr^{3+}-like behaviour and denoted by *, $\triangle$ and $\Diamond$. (The transitions are labelled as in Dunn *et al* 1986.) It was suggested that, for magnetic fields less than 0.3 T, the resonances denoted by * and $\triangle$ could arise from substitutional Cr^{3+} ions in (tetragonally) strain-stabilized sites. However, for fields above 0.3 T, it can be seen from figure 1 that strain stabilization does not occur as

the curves calculated for the two non-zero values of the strain do not coincide. Nevertheless, the resonances * and △ *are* observed and appear to correspond to the calculated curves for which the strain is between 0 and -20 cm^{-1}. Meanwhile, those experimental data points denoted by ◊ in figure 1 for the case when the magnetic field is close to or along the [111] direction were attributed to Cr^{3+} ions in zero-strained sites.

In the previous paper by Houbloss *et al* (1987), the intensity changes in the TD-EPR signals attributed to the Cr^{3+} centre, after sub-band-gap illumination, were rather small. It is therefore impossible to state that there is a definite correlation between the photo-induced effects on the 1.03 eV ZPL and the *, △, and ◊ resonances. In addition, the TD-EPR experimental data show some discrepancies with the calculated isofrequency curves. In this paper, we present the results of new experiments showing that the correlation noted previously between the observed TD-EPR spectra and the ZPL lines cannot now be sustained. We also describe in detail a strain-stabilized orthorhombic JT model for the system. Values for the parameters appearing in this model are deduced which give an entirely satisfactory account of the experimental data.

2.2. Energies of the impurity levels

The first Cr^{2+}/Cr^{3+} acceptor level lies 1.2 eV below the conduction band minimum and the second Cr^{+}/Cr^{2+} acceptor level is 0.5 eV below the conduction band minimum (Clerjaud 1985). The P antisite is a double donor such that the $+/++$ level has energy 1.25 eV above the top of the valence band and $0/+$ is located between E_c–0.8 eV and E_c–1.6 eV (Landolt–Börnstein 1989). As the paramagnetic state is seen in the dark, the centre should not have a negative U and thus the $0/+$ level should have a higher energy than the $+/++$ level.

3. Results from new TD-EPR experiments

A number of additional TD-EPR experiments have been carried out at liquid helium temperatures on further samples of semi-insulating GaP crystals, which were intentionally or accidentally doped with chromium. Measurements were made with the magnetic field $\boldsymbol{B}$ rotated in the $(1\bar{1}0)$, (001) and (111) planes at a frequency of 9.3 GHz. Details of these experiments, including the effects of sub-band-gap illumination, and the corresponding results obtained are described in this section.

3.1. Samples

Three types of chromium-doped sample of GaP have been studied in which the Fermi level is situated below (sample D), at (samples E) or above (samples Cr–S) the isolated Cr^{2+}/Cr^{3+} level. (Note that the latter samples are co-doped with sulphur.) TD or conventional OA spectra exhibit:

(a) only the 1.03 eV ZPL, indicating the presence of isolated Cr^{3+} ions in sample D,

(b) both the 1.03 and 0.87 eV ZPLs in samples E showing that they contain both the isolated Cr^{3+} and Cr^{2+} ions and

(c) only the Cr^{2+} 0.87 eV ZPL in the Cr–S samples.

In addition, GaP samples doped with other transition metals have also been examined; it is possible that chromium can be present in some of these samples as a contaminant.

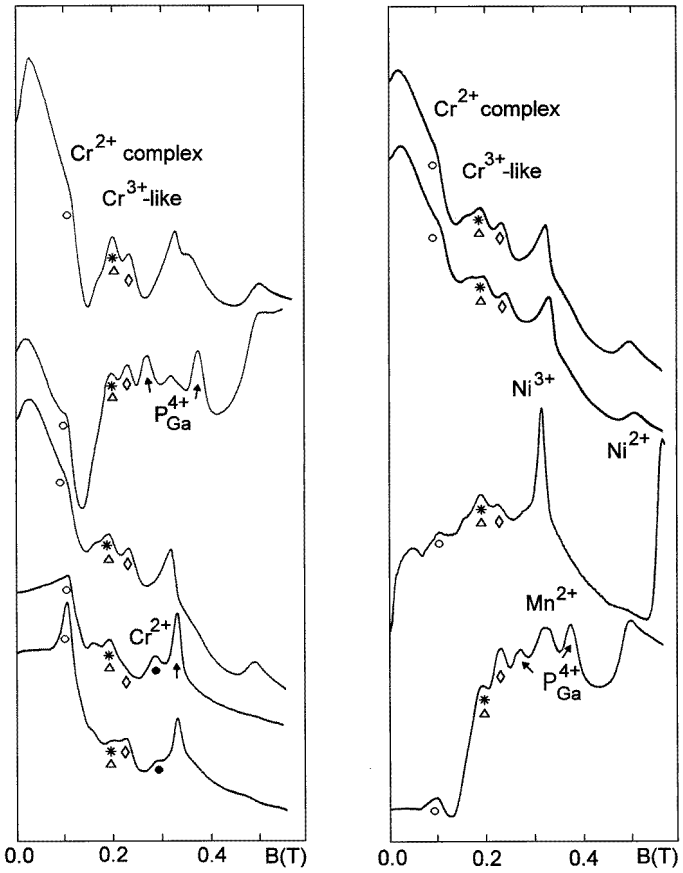

Figure 2. Typical TD-EPR spectra at a frequency of 9.3 GHz for $\boldsymbol{B}$ along the (111) axis. The signals from the Cr^{2+} complex are denoted by ○, from the isolated Cr^{2+} ion by ● and from the Cr^{3+}-like centres by *, △ and ◇. In (a), the three upper traces give results from three different GaP:Cr samples and the two lower traces are from the GaP:Cr:S samples placed in different positions in the microwave field in the as-received state. In (b), the upper trace is from the GaP:Cr (sample E) before illumination and the trace immediately below that is from the same sample after illumination. The lowest trace is from the GaP:Mn sample and the remaining trace is from the GaP:Ni sample.

In the TD-EPR spectra from all samples described above, we have searched for the lines which correspond to those which were labelled originally by *, △ and ◇ in Dunn *et al* (1986). When these resonances *are* observed, further detailed investigations of the effect of sub-band-gap illumination on their intensities have been undertaken. The TD-EPR spectra for $\boldsymbol{B}$ along [111] obtained from six of the many samples studied are shown in figure 2 for comparison.

3.2. Results from chromium-doped samples

The *, △ and ◇ resonances are *not* observed in sample D, which is expected to contain only isolated Cr^{3+}, while they *are* detected in the other chromium-doped samples which contain either both Cr^{2+} and Cr^{3+} or only Cr^{2+}. Figure 2(a) gives the spectra at 9.3 GHz with $\boldsymbol{B}$

along the [111] direction; the * and △ signals coincide for this orientation. The three upper curves are from different specimens doped only with chromium, which generate both the 0.87 and 1.03 eV ZPLs. The two lowest curves are obtained from a sample co-doped with chromium and sulphur for different positions in the r-f fields. It can be seen that the intensities of the Cr^{3+}-like resonance lines depend upon the geometry relative to the magnetic fields. The spectra from Cr–S crystals also exhibit signals due to Cr^{2+} (see figure 2(a)). In particular, it must be stressed that the *, △ and ◇ resonances do occur in the latter sample (Cr–S) in which there is no optical Cr^{3+} signal. Therefore the first point to note from these results is that the *, △ and ◇ lines cannot be due to the isolated substitutional Cr^{3+} ion.

Furthermore, new experiments examining the effects of illumination on these resonances are in agreement with this conclusion. In the samples investigated previously, the behaviour of the *, △ (below 0.3 T) and ◇ resonances was not always obvious due to the overlapping of the original resonances and the weakness of the effect. However, further experiments on samples E clearly show a decrease in the intensities of the TD-EPR Cr^{3+}-like resonances following illumination. This result is in contradiction with that expected if the *, △ and ◇ signals were from the Cr^{3+} ion, because, in these samples, the ZPL attributed to Cr^{3+} increases in intensity after illumination whilst both the Cr^{2+} ZPL and TD-EPR lines decrease. Figure 2(b) shows an example of TD-EPR spectra before and after illumination in sample E. It has been found that illumination has only a small effect on the resonances in the Cr–S samples.

It is also worth noting that the * and △ peaks have been studied mainly in fields lower than 0.3 T, corresponding to the strain-stabilized conditions of the Dunn *et al* (1986) theory. However, as stated previously, these two resonances having sharp peaks can often be detected much above 0.3 T and seem to correspond to a particular value of strain (~ -20 cm^{-1}) in the original model. These resonances are much more easily seen because they are more separated from other lines due to the higher values of the magnetic field. Consequently, it is easy to confirm that their intensities decrease after illumination in agreement with their low-field behaviour.

3.3. Results from GaP samples doped with other transition elements

Many other TD-EPR spectra from GaP samples doped with other transition elements (such as titanium, vanadium, manganese, iron, cobalt and nickel) have been examined in attempts to check whether the *, △ and ◇ resonances lines are really related to chromium. These lines are indeed also observed in samples doped with nickel or manganese; this is shown in figure 2(b) for $\boldsymbol{B}$ along the [111] axis. However, they have *not* been detected in any samples doped with other elements. At first sight, their presence in samples doped with nickel and manganese appears worrying. However, the TD-EPR spectra from the latter samples also exhibit very clearly the lines attributed by Bates *et al* (1984) to a Cr^{2+} complex (figure 2(b)). Furthermore, TD-EPR spectra obtained at fields above 2 T show a line attributed to the isolated Cr^{2+} ion (Vasson *et al* 1994). In the chromium-doped GaP sample investigated, this resonance is very large. However, in the spectra of the GaP samples doped with nickel or manganese and which exhibit the Cr^{3+}-like signals, the Cr^{2+} line is very weak indicating a concentration equal to or less than 10^{14} cm^{-3}. This suggests that the resonances, which are impurity related, could involve chromium.

From these results, we conclude that the centre responsible for the *, △ and ◇ resonances in the TD-EPR spectra shown above is *not* the same as the centre responsible for the 1.03 eV ZPL and therefore that it is not the isolated Cr^{3+} ion. However, it appears to be present together with the Cr^{2+}-related complex (denoted by ○ in figure 2) and is Cr^{3+}-like.

3.4. Measurements with conventional EPR

A recent examination of spectra obtained by conventional EPR on many of the same samples of GaP:Cr has not produced any information additional to that described above from TD-EPR.

4. Analysis of the TD-EPR experimental data

In this section, it will be shown that the experimental data shown in figures 3–5 are compatible with a Cr^{3+}-like centre having orthorhombic symmetry. The most general spin Hamiltonian for an $S = 3/2$ system can be written in the form:

$$\mathcal{H} = \mu_B \sum_{i,j} B_j g_{ji} S_i + \sum_{i,j} S_j D_{ji} S_i. \tag{4.1}$$

In the case of orthorhombic symmetry with the $\boldsymbol{g}$ and $\boldsymbol{D}$ tensors having the same principal axes X, Y and Z, the field-independent part of $\mathcal{H}$ can be written in the traceless form:

$$\mathcal{H} = D\left[S_z^2 - \frac{S(S+1)}{3}\right] + E(S_X^2 - S_Y^2). \tag{4.2}$$

The relation between the coefficients in (4.1) and (4.2) is: $D = \frac{3}{2}D_{ZZ}$ and $E = \frac{1}{2}(D_{XX} - D_{YY})$.

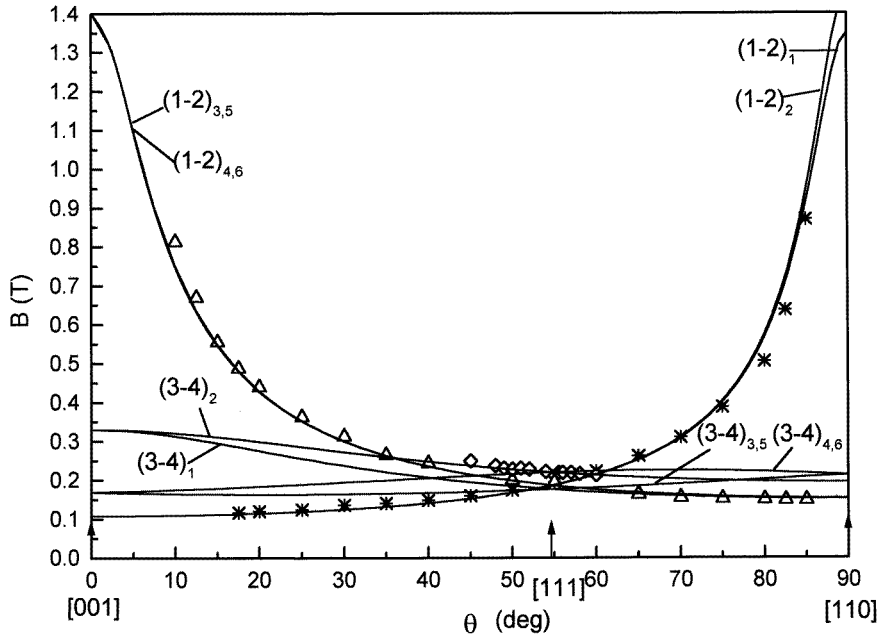

Figure 3. The calculated isofrequency curves (calculated with the theory given in section 5) and the corresponding experimental points (described in section 3) for $\boldsymbol{B}$ in the $(1\bar{1}0)$ plane at a frequency of 9.3 GHz.

If we define Z along the [001] axis, X along the [110] axis and Y along the $[\bar{1}10]$ axis for one of the orthorhombic centres (with the appropriate rotations for other physically

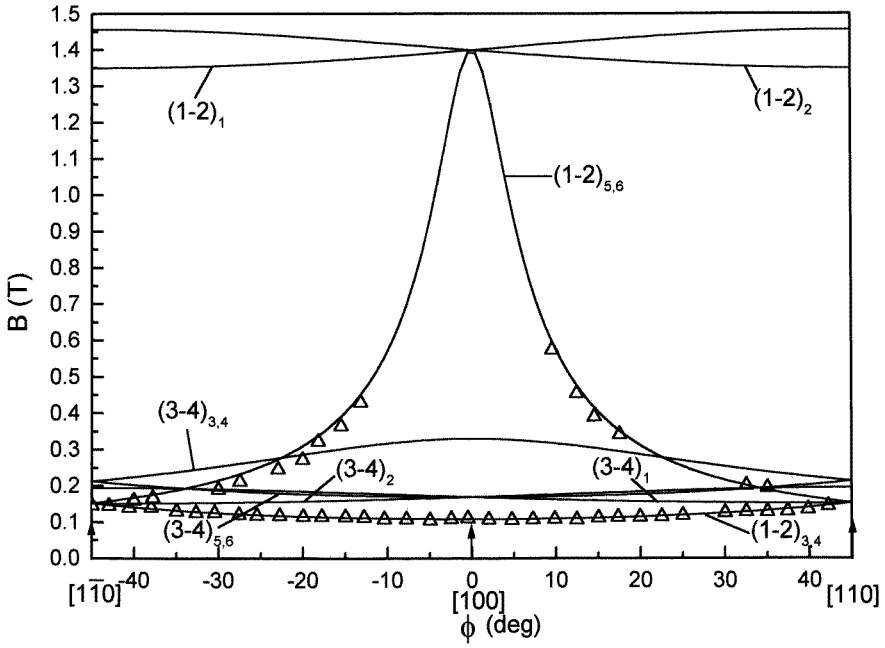

Figure 4. As figure 3 for the (001) plane.

equivalent centres), the experimental data of figures 3–5 can fit the Hamiltonians (4.1) and (4.2) with:

$$g_{ZZ} = 2.08 \qquad g_{XX} = 2.03 \qquad g_{YY} = 1.93 \qquad D = -1.7 \text{ cm}^{-1}$$
$$E = 0.147 \text{ cm}^{-1}. \tag{4.3}$$

The values of the parameters reported in (4.3) have been obtained by a computer fit, which diagonalized the 4×4 matrices for the six sites, to the isofrequency data displayed in figure 3 for $\boldsymbol{B}$ in the $(1\bar{1}0)$ plane. The fitting procedure involved calculating the resonant fields as a function of θ for all transitions between the energy levels labelled 1–4 (where 1 is lowest in energy etc) and identifying the sites and transitions simultaneously. The values of the parameters obtained generate the isofrequency graphs shown in figure 3. The same parameter values were used to *predict* the isofrequency curves in the (001) and (111) planes of figures 4 and 5; the fit of the calculated isofrequency curves to the experimental data appears to be entirely satisfactory. Further calculations show that the fourfold spin state is split into two doublets in zero field which are separated by 3.4 cm^{-1}. Thus the 3–4 transitions ($\Diamond$) are expected to be relatively weak because of depopulation effects. This is observed.

In order to gain further insight into the nature of the centre which generates the observed resonances, we develop in the next section a strain-stabilized orthorhombic JT model upon which the experimental data can be tested directly.

5. A $\mathbf{T_1 \otimes (e \oplus t_2)}$ JT model for the $\mathbf{Cr^{3+}}$-like centre

It is clear that the tetragonal JT model as given in Dunn *et al* (1986) does not give a satisfactory explanation of the Cr^{3+}-like data described here. On the other hand, the TD- and conventional EPR spectra from Cr^{3+} ions in GaAs have been modelled successfully

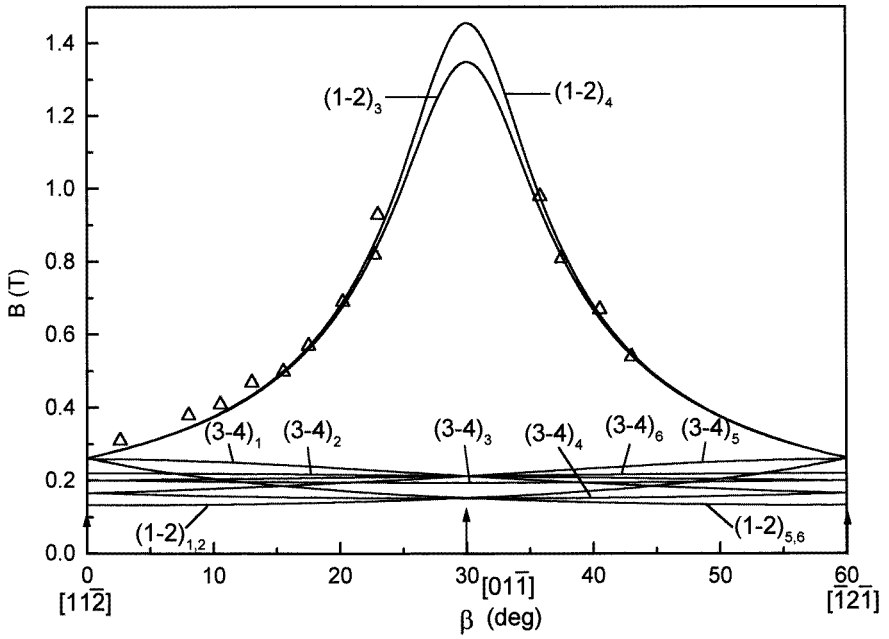

Figure 5. As figure 3 for the (111) plane.

by an orthorhombic strain-stabilized JT model by Parker *et al* (1990). In addition, the spectrum itself has orthorhombic symmetry as shown in the previous section. We note also that an orthorhombic Cr^{3+} centre in GaP was proposed by Butler *et al* (1987, 1989) in order to account for their phonon scattering experiments. Consequently, a strain-stabilized orthorhombic $T \otimes (e \oplus t_2)$ JT model will be developed in this section for the $^4T_1$ ground state, described by the isomorphic orbital operator $l = 1$, and tested against the TD-EPR results described above.

A rigorous model for the Cr^{3+}-like centre should use a JT model related to the point group of the complex in which the triplet electronic and vibrational modes are split. This represents a very complicated problem to be solved. However, the effective non-cubic part of the crystal field is expected to be smaller than the JT energy so that it is sufficient to set up the JT problem in cubic symmetry. (The neglect of the non-cubic part of the crystal field has been a very convenient and good approximation in other cases; see, for example, Clerjaud 1985, Bates and Stevens 1986 and Lacroix *et al* 1979). We suppose that the system is dominated by the vibronic coupling and that other interactions including the spin–orbit coupling ($\lambda \boldsymbol{l} \cdot \boldsymbol{S}$), the Zeeman terms for the magnetic field $\boldsymbol{B}$ and random strains etc can be treated as perturbations. In this so-called dynamic JT model, these perturbations may be described by effective Hamiltonians containing reduction factors which multiply the original electronic perturbations.

5.1. Derivation of the effective Hamiltonian

We suppose that a purely electronic perturbation can be expressed in the form

$$\mathcal{H}^{(1)} = \sum_{\Gamma\gamma} C_{\Gamma\gamma} L_{\Gamma\gamma} \tag{5.1}$$

where $C_{\Gamma\gamma}$ are coefficients which have symmetry Γ (and components γ) of the perturbation $\mathcal{H}^{(1)}$ and $L_{\Gamma\gamma}$ are electronic orbital operators having matrix elements in the electronic basis state $|\Sigma\sigma_i)$ identified by the Clebsch–Gordan (CG) coefficients from the relation $(\Sigma\sigma_i|L_{\Gamma\gamma}|\Sigma\sigma_j) = \langle\Gamma q_\gamma \Sigma\sigma_j|\Sigma\sigma_i\rangle$. The perturbation Hamiltonian (5.1) operates within the vibronic basis states. A general form of the effective Hamiltonian up to second order is (Polinger *et al* 1991)

$$\mathcal{H}_{eff} = \mathcal{H}^{(1)}_{eff} + \mathcal{H}^{(2)}_{eff} \tag{5.2}$$

where

$$\mathcal{H}^{(1)}_{eff} = \sum_{\Gamma\gamma} C_{\Gamma\gamma} K^{(1)}(\Gamma) L_{\Gamma\gamma} \tag{5.3}$$

$$\mathcal{H}^{(2)}_{eff} \sum_{\Gamma\gamma} \sum_{\Gamma_k\gamma_k} \sum_{\Gamma_l\gamma_l} C_{\Gamma_k\gamma_k} C_{\Gamma_l\gamma_l} \langle\Gamma_k\gamma_k\Gamma_l\gamma_l|\Gamma\gamma\rangle K^{(2)}_\Gamma(\Gamma_k \otimes \Gamma_l) L^{(2)}_{\Gamma\gamma} \tag{5.4}$$

and where $K^{(1)}(\Gamma)$ and $K^{(2)}_\Gamma(\Gamma_k \otimes \Gamma_l)$ are the first- and second-order reduction factors respectively. $L^{(2)}_{\Gamma\gamma}$ is a coupled electronic operator:

$$L^{(2)}_{\Gamma\gamma} = \sum_{\gamma_k\gamma_l} L_{\Gamma_k\gamma_k} L_{\Gamma_i\gamma_i} \langle\Gamma_k\gamma_k\Gamma_l\gamma_l|\Gamma\gamma\rangle. \tag{5.5}$$

For fixed Γ_k and Γ_l, the second-order effective Hamiltonian is reduced to

$$\mathcal{H}^{(2)}_{eff} = \sum_{\Gamma\gamma} K^{(2)}_\Gamma(\Gamma_k \otimes \Gamma_l) S^{(2)}_{\Gamma\gamma} L^{(2)}_{\Gamma\gamma} \tag{5.6}$$

where

$$S^{(2)}_{\Gamma\gamma} = \sum_{\Gamma\gamma} C_{\Gamma_k\gamma_k} C_{\Gamma_l\gamma_l} \langle\Gamma_k\gamma_k\Gamma_l\gamma_l|\Gamma\gamma\rangle. \tag{5.7}$$

As an example of the application of the above formulae, we consider the perturbation Hamiltonian

$$\mathcal{H}^{(1)} = 2\mu_B \boldsymbol{B}\cdot\boldsymbol{S} + \boldsymbol{l}\cdot(\lambda\boldsymbol{S} + \mu_B\boldsymbol{B}) \tag{5.8}$$

where λ is the spin–orbit coupling constant and μ_B is the Bohr magneton. Comparing (5.8) with the general form of $\mathcal{H}^{(1)}$ given in (5.1), we have

$$\begin{aligned} &L_{A_1} = I \qquad C_{A_1} = 2\mu_B \boldsymbol{B}\cdot\boldsymbol{S} \\ &L_{T_i\gamma} = \frac{\mathrm{i}}{\sqrt{2}} l_\gamma \qquad C_{T_1\gamma} = -\mathrm{i}\sqrt{2}(\lambda S_\gamma + \mu_B B_\gamma) \qquad (\gamma = x, y, z). \end{aligned} \tag{5.9}$$

On substituting (5.9) into (5.5) and (5.7), we obtain

$$L^{(2)}_{\Gamma\gamma} = -\frac{1}{2} \sum_{\Gamma_k\gamma_l} l_{\gamma_k} l_{\gamma_l} \langle T_1\gamma_k T_1\gamma_l|\Gamma\gamma\rangle \tag{5.10}$$

and

$$S^{(2)}_{\Gamma\gamma} = -2\lambda^2 \sum_{\Gamma_k\gamma_l} S_{\gamma_k} S_{\gamma_l} \langle T_1\gamma_k T_1\gamma_l|\Gamma\gamma\rangle - 2\lambda\mu_B \sum_{\gamma_k\gamma_l} (B_{\gamma_k} S_{\gamma_l} + B_{\gamma_l} S_{\gamma_k}) \langle T_1\gamma_k T_1\gamma_l|\Gamma\gamma\rangle. \tag{5.11}$$

In (5.11), we have dropped the terms quadratic in B. The values of the CG coefficients in the above formulae depend upon the symmetry of the system.

We suppose that the Hamiltonian is invariant under the cubic T_d group. Therefore, using (5.3)–(5.11) and inserting the corresponding CG coefficients, we can rewrite the effective Hamiltonian as

$$\mathcal{H}_{eff} = 2\mu_B(\boldsymbol{B}\cdot\boldsymbol{S}) + K^{(1)}(T_1)\boldsymbol{l}\cdot(\lambda\boldsymbol{S} + \mu_B\boldsymbol{B}) + \lambda^2[\tfrac{1}{3}K^{(2)}_{A_1} l(l+1)S(S+1)$$

$$+\tfrac{2}{3}K_E^{(2)}\boldsymbol{E}(l)\cdot\boldsymbol{E}(S)-\tfrac{1}{2}K_{T_1}^{(2)}\boldsymbol{l}\cdot\boldsymbol{S}+\tfrac{2}{3}K_{T_2}^{(2)}\boldsymbol{T}(l)\cdot\boldsymbol{T}(S)]$$
$$+\lambda\mu_B[\tfrac{2}{3}K_{A_1}^{(2)}(\boldsymbol{B}\cdot\boldsymbol{S})l(l+1)+\tfrac{4}{3}K_E^{(2)}\boldsymbol{E}(l)\cdot\boldsymbol{E}(SB)+\tfrac{4}{3}K_{T_2}^{(2)}\boldsymbol{T}(l)\cdot\boldsymbol{T}(SB)] \tag{5.12}$$

where $\boldsymbol{E}$ and $\boldsymbol{T}$ are tensor operators which are defined as (O'Brien 1990)

$$\begin{aligned}&\boldsymbol{E}(l)=\{E_\theta^l,E_\varepsilon^l\} && T(l)=\{T_{yz}^l,T_{zx}^l,T_{xy}^l\}\\ &\boldsymbol{E}(S)=\{E_\theta^S,E_\varepsilon^S\} && T(S)=\{T_{yz}^S,T_{zx}^S,T_{xy}^S\}\\ &\boldsymbol{E}(SB)=\{E_\theta^{SB},E_\varepsilon^{SB}\} && T(SB)=\{T_{yz}^{SB},T_{zx}^{SB},T_{xy}^{SB}\}\end{aligned} \tag{5.13}$$

with the component electronic operators given, for example, by

$$\begin{aligned}&E_\theta^l=\frac{1}{2}[3l_z^2-l(l+1)] && E_\varepsilon^l=\frac{\sqrt{3}}{2}[l_x^2-l_y^2] && T_{yz}^l=\frac{\sqrt{3}}{2}[l_yl_z+l_zl_y]\\ &E_\theta^{SB}=\frac{1}{2}[3S_zB_z-SB] && E_\varepsilon^{SB}=\frac{\sqrt{3}}{2}[S_xB_x-S_yB_y] && T_{yz}^{SB}=\frac{\sqrt{3}}{2}[S_yB_z+S_zB_y].\end{aligned} \tag{5.14}$$

The component operators for $\boldsymbol{E}(S)$ and $\boldsymbol{T}(S)$ are obtained from those of $\boldsymbol{E}(l)$, $\boldsymbol{T}(l)$ by replacing l with S.

5.2. The spin Hamiltonian with stress

In the effective Hamiltonian (5.12), the effect of strain has been ignored. However, if the impurity ion is placed in a real crystal, it is necessary to include strain terms in the Hamiltonian in order to explain the experimental data. As the JT model used reflects orthorhombic symmetry, we will suppose that the strains are dominated also by those of orthorhombic symmetry in the following discussions. The effective orthorhombic strain Hamiltonian for a site labelled 1 of symmetry [110] is given by

$$\mathcal{H}_s^{[110]}=-\tfrac{1}{2}\bar{V}_E\bar{Q}_\theta E_\theta^l+\tfrac{3}{2}\bar{V}_T\bar{Q}_6T_{xy}^l \tag{5.15}$$

where $\bar{V}_E$ and $\bar{V}_T$ are equal to V_E and V_T multiplied by appropriate first-order reduction factors, and $\bar{Q}_\theta$ is the static contribution to Q_θ from static strains of E_θ-type symmetry etc. This strain Hamiltonian has C_{2v} symmetry so that the degeneracy of the ground T_1 triplet state is lifted. Its energies E_i and the corresponding eigenstates are found to be

$$\begin{aligned}&E_1=-\frac{1}{4}[\bar{V}_E\bar{Q}_\theta+3\sqrt{3}\bar{V}_T\bar{Q}_6] && |\phi_1\rangle=\frac{1}{\sqrt{2}}|x+y\rangle\\ &E_2=-\frac{1}{4}[\bar{V}_E\bar{Q}_\theta-3\sqrt{3}\bar{V}_T\bar{Q}_6] && |\phi_2\rangle=\frac{1}{\sqrt{2}}|x-y\rangle\\ &E_3=-\frac{1}{2}\bar{V}_E\bar{Q}_\theta && |\phi_3\rangle=|z\rangle\end{aligned} \tag{5.16}$$

where $E_1<E_2<E_3$.

The same analysis can be carried out for the strains along the other five directions, namely $[1\bar{1}0]$, [011], $[01\bar{1}]$, [101] and $[\bar{1}01]$, which generate the sites labelled 2–6 respectively, with results which differ only in some signs. From (5.16), it can be seen that the effect of the orthorhombic strain is to lower the energy of one of the wells relative to the other wells. The result is that the whole system will be locked into the well of lowest energy and show orthorhombic properties. Therefore, the spin Hamiltonians describing this system can be obtained by simply averaging the effective Hamiltonians (5.12) over

the ground states $|\phi_1\rangle$ of the strain Hamiltonians. Dropping a constant term, the spin Hamiltonian ($S = 3/2$) for the [110] site can be written as (Vasson *et al* 1997)

$$\mathcal{H} = D[S_z^2 - \tfrac{1}{3}S(S+1)] + g_\parallel \mu_B B_z S_z + g_\perp \mu_B (B_x S_x + B_y S_y) + E(S_x S_y + S_y S_x) + F\mu_B (B_x S_y + B_y S_x) \tag{5.17}$$

where

$$g_\parallel = 2 + \tfrac{1}{3}\lambda(4K_{A_1}^{(2)} + 2K_E^{(2)}) \qquad g_\perp = 2 + \tfrac{1}{3}\lambda(4K_{A_1}^{(2)} - K_E^{(2)})$$
$$D = \tfrac{1}{2}\lambda^2 K_E^{(2)} \qquad E = -\tfrac{1}{2}\lambda^2 K_{T_2}^{(2)} \qquad F = -\lambda^2 K_{T_2}^{(2)}. \tag{5.18}$$

A $\pi/4$ rotation around the $z = Z$ axis converts the Hamiltonian (5.17) into the Hamiltonians (4.1) and (4.2). The correspondence between the symbols is:

$$g_{ZZ} = g_\parallel \qquad g_{XX} = g_\perp + F \qquad g_{YY} = g_\perp - F. \tag{5.19}$$

6. Discussion and conclusions

The main conclusion to be drawn from these results is that the correlation between the 1.03 eV ZPL of the isolated Cr^{3+} ion in GaP and the TD-EPR data reported previously can no longer be supported. The orthorhombic JT model is shown to give a very satisfactory account of all the data but is nevertheless insufficient to give direct information on the nature of the centre itself. In particular, it can be seen that the fit of the calculated curves to the experimental data points shown in figures 3–5 is entirely satisfactory. The spin Hamiltonian (5.17) which is appropriate for a strain-stabilized orthorhombic JT system has been used successfully to explain the TD-EPR experimental results for the GaP:Cr^{3+}-like system. This model has one additional advantage over the tetragonal JT model used previously; some of the resonances (e.g. those in the region of $B = 0.2$ T when B is close to the [111] direction as shown in figure 1 by the symbol $\Diamond$) all have strain-stabilized counterparts. There is therefore no longer a need to introduce zero strain to explain the experimental data observed with this high-symmetry direction of the magnetic field.

There is an even more significant feature arising from the values obtained for the spin Hamiltonian parameters using the new model. In both the original and recent experiments, a very intense line was frequently observed for $\boldsymbol{B}$ along the $\langle 001 \rangle$ directions for $B = 1.4$ T, with an intensity which decreased rapidly as $\boldsymbol{B}$ was moved away from the symmetry axis. Figure 4, for example, provides a simple explanation; with the field directed precisely along this direction for which $\phi = 0$, four of the transitions within the lower doublet exactly coincide with a consequent maximum in the observed intensity. As ϕ is increased or decreased, two of the transitions (5 and 6) occur at a rapidly reducing field whereas the two other transitions (1 and 2) remain close to 1.4 T. The overall effect is a marked decrease in the strength of the TD-EPR signal as observed. This provides further evidence that the very strong line at 1.4 T is indeed from this Cr^{3+}-like centre.

The relative intensities of the Cr^{3+}-like resonances are sample dependent. This is expected because the relative intensities depend upon the number of sites satisfying the strain-stabilized condition for that resonance and this will vary with the sample as seen in figure 2(a). There is a further complication in that the TD-EPR technique gives very strong resonances from electric-field-induced transitions and they can dominate the magnetic-field-induced transitions. The proportion of the signal from each depends upon the position of the sample in the cavity and on its size and thus these additional factors also affect the relative intensities of the resonances between different samples as observed.

To gain further insight into the nature of the JT coupling in this system, it is necessary to calculate values for the second-order reduction factors. Using the expressions for $g_{\|}$, $g_{\perp}$ and F given in (5.18) and the numerical values given in (4.3), we obtain:

$$K_{T_2}^{(2)} \approx -6.23 \times 10^{-4}(\mathrm{cm}^{-1})^{-1} \qquad K_E^{(2)} \approx 1.2 \times 10^{-3}(\mathrm{cm}^{-1})^{-1}$$
$$K_{A_1}^{(2)} \approx 1.2 \times 10^{-4}(\mathrm{cm}^{-1})^{-1}.$$

First- and second-order reduction factors for the orthorhombic system have been calculated previously by Dunn and Bates (1989) and by Hallam *et al* (1992). The results obtained there are reproduced in figure 6 (note that, in this figure, the second-order reduction factors in the form $K_1^{(2)}\bar{h}\omega$ are plotted as a function of $K_T/\bar{h}\omega$). Taking $\bar{h}\omega = 200$ cm^{-1}, we find that $K_{T_2}^{(2)}/\bar{h}\omega \approx -0.125$ is obtained. This value corresponds approximately to $K_T/\bar{h}\omega \approx 1.7$ as indicated by the arrow in figure 6. This result implies that the Cr^{3+}-like centre in GaP is a strongly coupled orthorhombic Jahn–Teller centre. The values of $K_B^{(2)}$ and $K_{A_2}^{(2)}$ are also small but they appear here with wrong signs. This is not surprising, because the effective Hamiltonian (5.12) has been developed by a consideration of the coupling to the excited vibronic states only. Thus, the expressions given in equation (5.18) can have only qualitative validity. Further improvement can be made by considering admixtures of the excited electronic states into the $^4T_1$ ground state via spin–orbit coupling (Parker *et al* 1990). However, since other quantitative information on this Cr^{3+}-like centre in GaP is unavailable, further calculations of contributions from these kinds of admixture would not be meaningful and so will not be considered further in this paper.

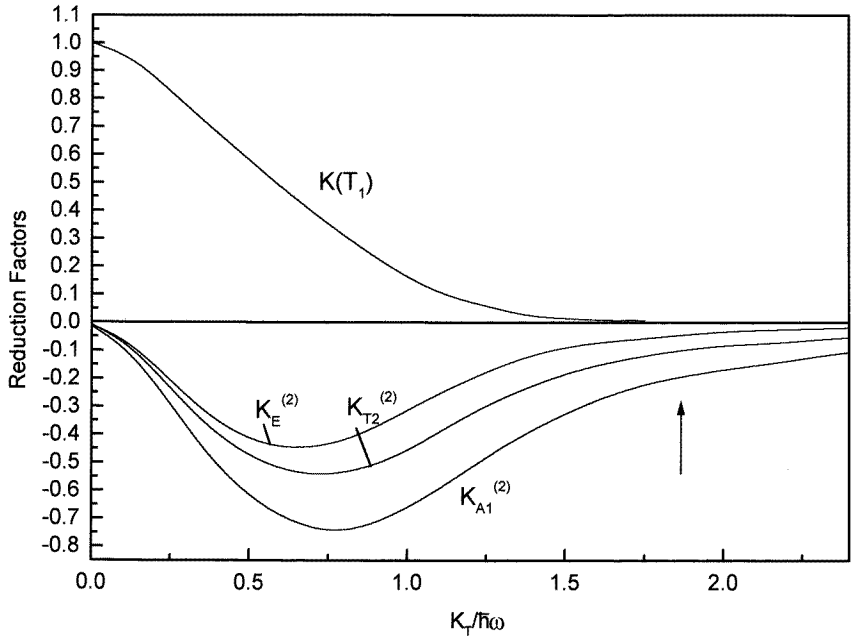

Figure 6. First- and second-order reduction factors as a function of the strength of the vibronic coupling strength as calculated by Dunn and Bates (1989) and Hallam *et al* (1992). The arrow denotes the value chosen to fit the experimental data.

Despite these difficulties, we note that any further modifications to equation (5.18) will not affect our main conclusion that the Cr^{3+}-like centre in GaP is a strongly coupled

orthorhombic JT centre. However, such modification may change slightly the magnitudes and/or reverse the signs of the second-order reduction factors. It is very clear from figure 6 that in the weak- and intermediate-JT-coupling regions, the first-order reduction factor $K^{(1)}(T_1)$ dominates the second-order factors. However, in the case of the centre considered here, the role played by the first-order reduction factors is small but it cannot be totally ignored. Consequently, in order to include first-order reduction factors in the fitting procedures, extra terms must be added to the expressions (5.18) by taking into account off-diagonal matrix elements between the basis states of the strain Hamiltonian. Alternatively, the effective Hamiltonians (5.12) and (5.15) may be used to fit the experimental data. Nevertheless, the fact that the spin Hamiltonian (5.17) fits our TD-EPR data indicates that the Cr^{3+}-like centre in GaP is indeed a strongly coupled JT system.

The literature contains reference to two other low-symmetry Cr^{3+} centres which have been observed in GaP by EPR (Kaufmann and Schneider 1982, Kreissl *et al* 1992). The centre described here is different and has been described as 'Cr^{3+}-like' because it has been modelled by a spin of $\frac{3}{2}$ and it is only present in samples containing chromium. In particular, it is only present in samples in which chromium is also present in the Cr^{2+} state. One possibility could be that the centre is formed by a Cr^{2+} ion adjacent to an antisite having a spin of $\frac{1}{2}$. A spin of $\frac{3}{2}$ could then arise through the coupling of the two spins of 2 and $\frac{1}{2}$ by an exchange-type mechanism. The major argument against this suggestion is that the centre would be expected to possess a pronounced trigonal symmetry which is *not* observed. It is possible that the trigonal field arising in either model is smaller in magnitude than anticipated because of quenching by the JT effect itself as discussed earlier. However, the modelling described above is largely based on a near-tetrahedral environment for the Cr^{3+}-like centre. This makes this centre very similar to the isolated substitutional Cr^{3+} ion in GaAs which is also strongly coupled and subject to an orthorhombic $T \otimes (e \oplus t_2)$ JT effect but without an identifiable ZPL. Unfortunately, the nature of the electronic structure of this centre remains unresolved.

The electronic structure of transition metal ions in GaAs and in InP was essentially solved about 15 years ago (apart from detailed refinements added later) as reviewed, for example, by Clerjaud (1985). In contrast, GaP remains a very different type of host for transition metal ions and many problems remain. In addition to the Cr^{3+}-like centre described here, a very recent analysis by Al-Shaikh *et al* (1998) of the Ti^{3+} centre in GaP has highlighted the difficulties of our lack of understanding of this host when doped with impurities. The role of the JT effect in combination with random strains is important as it could have important consequences in the understanding the effects of impurities on the device properties.

Acknowledgments

The authors would like to acknowledge the many valuable discussions they have had with Professor W Ulrici on many aspects of this work and for the samples used in the experiments.

References

Al-Shaikh A M, Qui Q C, Roura P, Ulrici W, Clerjaud B, Bates C A and Dunn J L 1998 *J. Phys.: Condens. Matter* **10** 3367–86

Bates C A, Handley J, Vasson A and Vasson A-M 1984 *J. Phys. C: Solid State Phys.* **17** L603–6

Bates C A and Stevens K W H 1986 *Rep. Prog. Phys.* **49** 783–823

Butler N, Challis L J, Sahraoui-Tahar M, Salce B and Ulrici W 1987 *Japan. J. Appl. Phys.* **26** (Supplement) 675–6

——1989 *J. Phys.: Condens. Matter* **1** 1191–203
Clerjaud B 1985 *J. Phys. C: Solid State Phys.* **18** 3615–61
Darcha M, Vasson A. Vasson A-M, Bates C A and Dunn J L 1987 *J. Phys. C: Solid State Phys.* **20** 2261–9
Dean 1973 *J. Lumin.* **7** 51
Dunn J L and Bates C A 1989 *J. Phys.: Condens. Matter* **1** 2617–29
Dunn J L, Bates C A, Darcha M, Vasson A and Vasson A-M 1986 *Phys. Rev.* B **33** 2029–32
Eaves L, Englert T L, Uihlein Ch and Williams P J 1980 *J. Phys. Soc. Japan Suppl.* **49** 279–82
Eaves L, Halliday D P and Uihlein Ch 1985 *J. Phys. C: Solid State Phys.* **18** L449–52
Hallam L D, Dunn J L and Bates C A 1992 *J. Phys.: Condens. Matter* **4** 6797–810
Houbloss S, Nakib A, Vasson A, Vasson A-M, Bates C A, Dunn J L and Ulrici W 1987 *J. Phys. C: Solid State Phys.* **20** L467–73
Kaufmann U and Koschel W H 1978 *Phys. Rev.* B **17** 2081–4
Kaufmann U and Schneider J 1982 *Adv. Electron Electron Phys.* **58** 81–141
Krebs J J and Stauss G H 1977 *Phys. Rev.* B **15** 17–22
Kreissl J, Ulrici W, Rehse U and Gehlhoff W 1992 *Phys. Rev.* B **12** 2065–80
Lacroix R, Weber and Duval J E 1979 *J. Phys. C: Solid State Phys.* **18** L449–52
Landolt–Bornstein New Series 1989 Group III, vol 22b, 6th edn (Berlin: Springer)
O'Brien M C M 1990 *J. Phys.: Condens. Matter* **2** 5539–53
Parker L W, Bates C A, Dunn J L, Vasson A and Vasson A-M 1990 *J. Phys.: Condens. Matter* **2** 2841–56
Polinger V Z, Bates C A and Dunn J L 1991 *J. Phys.: Condens. Matter* **3** 513–27
Vasson A, Vasson A-M, Tebbal N, El-Metoui M and Bates C A 1993 *J. Phys. D: Appl. Phys.* **26** 2231–8
——1994 *Mater. Sci. Forum* **143–147** 833–8
Vasson A-M, Vasson A, Darcha M, Erramli A, El-Metoui, Liu Y M, Bates C A and Dunn J L 1997 *Z. Phys. Chem.* **201** 55–62
Williams P J, Eaves L, Simmonds P E, Henry M O, Lightowlers E C and Uihlein Ch 1982 *J. Phys. C: Solid State Phys.* **15** 1337–43